Premelting phenomena in pseudo-binary ionic crystals

2010 J. Phys.: Condens. Matter 22 155104

(http://iopscience.iop.org/0953-8984/22/15/155104)

J. Phys.: Condens. Matter **22** (2010) 155104 (11pp) doi:10.1088/0953-8984/22/15/155104

Premelting phenomena in pseudo-binary ionic crystals

Shigeki Matsunaga

Nagaoka National College of Technology, Nagaoka 940-8532, Japan

E-mail: matsu@nagaoka-ct.ac.jp

Received 10 August 2009, in final form 1 February 2010
Published 9 March 2010
Online at stacks.iop.org/JPhysCM/22/155104

Abstract

The theory of the premelting phenomena in ionic crystals on the basis of the concept of the heterophase fluctuation has been applied to the pseudo-binary ionic crystals, KCl–NaCl, AgBr–AgCl and AgBr–CuBr systems. Molecular dynamics simulations (MD) have been performed to examine the ionic configurations in their premelting region in the vicinity of their melting points. Liquid-like clusters have been observed in the results of MD utilizing the Lindemann instability condition. The sizes of liquid-like clusters have been estimated by theory and MD. The characteristics of the dynamical behavior of ions in the premelting region have been examined by the mean square displacement and the velocity correlation functions.

(Some figures in this article are in colour only in the electronic version)

1. Introduction

The anomalous temperature dependence of the physical properties of ionic crystals in the vicinity of melting point have been widely studied by experiment, such as ionic conductivity [1], specific heat [2], the thermal expansion coefficient [3], etc [4]. These premelting phenomena have been interpreted as the heterophase fluctuation, in other words the premelting consists of actual melting in the pure crystal in small regions of space and time near the melting point. This concept was proposed by Frenkel many years ago [5]. In previous studies, we have investigated the theoretical background of these anomalous premelting phenomena in ionic crystals. We have re-examined Frenkel's theory in relation to the thermodynamical model and the size of liquid-like clusters which may be formed in the ionic crystals. We have also performed molecular dynamics simulations (MD) in two different types of ionic crystals, namely silver halides, AgBr and AgCl, and alkali halides, NaCl and KCl, in order to confirm the theoretical results, especially the estimated size of liquid-like clusters. The results were in good agreement among themselves [6].

AgBr and AgCl have a rock salt structure in their solid phase, which does not exhibit superionic conduction to their melting temperature. On the other hand, AgI is one of the typical examples of a superionic conductor in its α phase, i.e. α AgI, where the diffusion coefficient of the Ag ion is of the same order as that of liquids. In α AgI, Ag ions move through the interstitial sites of the body centered cube of I ions [7]. Concerning this point, Andreoni and Tosi [8], and later Nield *et al* [9] suggested from the structural study that the disorder of Ag ions in the rock salt silver halides is observed before melting, and the feasible transition of AgBr and AgCl into the superionic phase seems to be prevented by melting. In our previous research, we have reported that Ag ions in silver halides in the premelting region show large deviation from their original lattice sites corresponding to experiment [6].

Meanwhile, we have also examined the pseudo-binary or ternary ionic crystals, e.g. noble metal halide mixtures and alkali halide mixtures as serial works. It is of particular interest to study the change of their physical properties by dissolving different types of silver halide AgBr or AgCl into AgI, and the reverse. In our previous works, we have carried out MD in molten silver halide mixtures to discuss the mixing effect on the structure and transport properties [10]. It is worth noting that the ratios of partial conductivities in ternary molten salts are found to be constant regardless of their temperature [10]. Since these phenomena were first found in binary molten salts their theoretical background has been investigated [11]. As an extension, we have also studied the dielectric screening effect in molten salts and their mixtures, i.e. the effective potential between cations and anions are significantly altered by the existence of the surrounding opposite ions [12]. The dielectric screening effect may affect the dynamical behavior of ions in molten salts. We have investigated the dynamics of ions in molten silver halide mixtures and found the ionic

vibration has pronounced peaks in the 'terahertz' region [13]. Furthermore, we have studied the superionic phase of AgBr–CuBr as an example of a system with two kinds of mobile cations, Cu^+ and Ag^+, to examine the distribution difference between cations [14].

Therefore, it seems as a matter of great importance to examine the various aspects of mixtures of ionic crystals. Regarding defect formation in ionic crystals, the formation free energy of a pair of Schottky-type defects was shown to be lowered by the appearance of a defect–defect interaction with increasing temperature using the Debye–Hückel approximation [15]. In connection with the specific heat data of ionic crystals, the correction term due to the defect–defect interaction was shown to be proportional to the cube root of the Frenkel-type defect concentration [16]. In recent years, the appearance of defect clusters in crystals has been analyzed by means of computer simulation using the Lindemann instability condition [17]. In this study, as a serial work, we apply the theory of liquid-like clusters in the premelting region to pseudo-binary ionic crystals, which are compared to MD results. The dynamical aspects of liquid-like clusters are also investigated by MD.

2. Defects and liquid-like clusters in ionic crystals

The theory of defect formation and liquid-like clusters in the premelting region has been developed by the reconstructed Frenkel theory and the theory of ionic conductivity. In the following sections, we will summarize the important results of the theory, obtained in the former articles, for the reader's convenience [6].

In this study, we denote this sort of liquid-like local cluster as the B′-state and the other parts keeping the condition of ordinal ionic crystal as the A-state. These clusters of B′-state can be created and annihilated dynamically in time and space, keeping the thermal equilibrium for A $\leftrightarrow$ B′ and indicating macroscopically as one phase. Hereafter we will call this sort of cluster the 'quasi-liquid', in short the 'L' state. One of our main purposes is to investigate whether its physical properties are similar to those of bulk liquid or not.

With increasing temperature, the lattice composed of the mixture of states A and B′ approaches the phase transition to the liquid state B. This change may be interpreted using the two steps transition model; transition 1 from the original state A to the mixture state A and B′, a kind of higher order transition like the order–disorder case; transition 2 being the usual melting of the system. It may be possible to define the chemical potential in the B′ cluster as $\mu_{B'}$. We also denote the chemical potential of the A-state as μ_A.

We consider an ionic crystal accompanied by a premelting dislocation in the vicinity of its melting point. We assume that the number of positive and negative ions are both equal to N, and the number density of the liquid state B and of B′-clusters are almost the same value n_0. The approximation $\mu_{B'} \sim \mu_B$ has been made. The most ideal shape of a B′-cluster containing s defect pairs that minimizes the surface energy is supposed to be a sphere, thus $s = n_0(4\pi r^3/3)$. The surface area of this sphere is given by $4\pi(3s/4\pi n_0)^{2/3}$, thus the surface free energy, α, is $4\pi\sigma(3s/4\pi n_0)^{2/3}$, where σ is the surface tension per unit area. The total chemical potential of this cluster is given by $(s\mu_B + \alpha s^{2/3})$. The total Gibbs free energy of the system G_{total} is described as follows,

$$G_{total} = N_A\mu_A + \Sigma_{s=s0} g_s(s\mu_B + \alpha s^{2/3}) + S_{mix}(g_s, T) \quad (1)$$

where N_A is the number of ion pairs belonging to the A-phase, g_s the total number of s-pairs clusters, and s_o the lowest number of ion pairs. $S_{mix}(g_s, T)$ stands for the mixing entropy, and its simplified expression is

$$S_{mix}(g_s, T) = k_B T[N_A \ln\{N_A/(N_A + \Sigma g_s)\} + \Sigma_s g_s \ln\{g_s/(N_A + \Sigma g_s)\}]. \quad (2)$$

The total number of ions N is kept constant, thus we have

$$\{N_A/(N_A + \Sigma g_s)\} = C\exp[-\beta\mu_A] \quad (3)$$

where $\beta = 1/k_B T$. We assume the total fraction of clusters to be much smaller in comparison with N, i.e., $\Sigma g_s \ll N_A \sim N$, then we have

$$g_s \cong N\exp[-\beta\{s(\mu_B - \mu_A) + \alpha s^{2/3}\}]. \quad (4)$$

The chemical potentials μ_A and μ_B satisfy the following relation at a temperature T just below the melting point T_m,

$$\mu_B - \mu_A = \{(\partial\mu_B/\partial T)_{Tm} - (\partial\mu_A/\partial T)_{Tm}\}(T - T_m) = -(L_m/NT_m)(T - T_m) \quad (5)$$

where L_m is the latent heat of fusion. Combining the above equations, we have the following relation

$$G_{total} = N\mu_A - Nk_B T\int_{s_0}^{\infty} \exp[-\beta\{s(L_m/NT_m)(T_m - T) + \alpha s^{2/3}\}]\,ds \quad (6)$$

where we have made the approximation to obtain (6) that the number of ion pairs s is continuous with its lowest value s_0. It is recognized from (6) that the Gibbs free energy of the system is lowered by the mixture of (A-state + B′-state) rather than the homogenized A-state. It means the appearance of the clusters indicated by B′-state is plausible from the viewpoint of the thermodynamic condition. Using the Gibbs–Helmholtz equation, the enthalpy change, ΔH, corresponding to the second term on the right-hand side of equation (6) is equal to

$$\Delta H = L_m\int_{s_0}^{\infty} s\exp[-\beta\{s(L_m/NT_m)(T_m - T) + \alpha s^{2/3}\}]\,ds. \quad (7)$$

The defects' fraction has been obtained in some ionic crystals by the anomalous temperature dependencies of specific heats accompanied by the Frenkel-type defect [8]. Applying the Maxwell relation to (7), we have the specific heat of the mixture system of A and B′ at the melting point, $C_p(T_m)$, as follows

$$C_p(T_m) = C_p^A(T_m) + (3/2)(L_m^2/Nk_B T_m^2) \times \left[(1/\beta\alpha)s_0^{7/3}\exp\{-\beta\alpha s_0^{2/3}\} + (17/6\beta\alpha) \times \int_{s_0}^{\infty} s^{4/3}\exp\{-\beta\alpha s^{2/3}\}\,ds\right] \quad (8)$$

where $C_p^{\mathrm{A}}(T_{\mathrm{m}})$ is the normal specific heat in the case that A-state only exists at the melting temperature T_{m}. There is a phenomenological but important relation, i.e. $\chi_T\alpha \sim L$, where L is a constant with the dimension of length [5, 18]. χ_T is the isothermal compressibility of the quasi-liquid B′-state, however, we use the value in molten phase at melting temperature. The value of L is about 0.35 A for most of the molten salts. Using this relation, we obtain $\beta\alpha \sim 1/7$. The normal specific heat of A-state, $C_p^{\mathrm{A}}(T)$, where only some defects distribute randomly, may be expressed by a linear temperature dependence. If we assume that the distribution of the cluster sizes is rather sharp around the value of $\hat{s}$, and close to the lowest one s_0, then we have the following form as an approximation of (8),

$$C_p(T_{\mathrm{m}}) \sim C_p^{\mathrm{A}}(T_{\mathrm{m}}) + (3/2)(L_{\mathrm{m}}^2/Nk_{\mathrm{B}}T_{\mathrm{m}}^2) \times [(1/\beta\alpha)\hat{s}^{7/3}\exp\{-\beta\alpha\hat{s}^{2/3}\}]. \quad (9)$$

Then the specific heat at the temperature T in the vicinity of the melting point, $C_p(T)$ is expressed as follows,

$$C_p(T) \sim C_p^{\mathrm{A}}(T_{\mathrm{m}}) + \Delta C_p(T_{\mathrm{m}})\exp[L_{\mathrm{m}}\hat{s}/Nk_{\mathrm{B}}T_{\mathrm{m}}] \times \exp[-L_{\mathrm{m}}\hat{s}/Nk_{\mathrm{B}}T] \quad (10)$$

where

$$\Delta C_p(T_{\mathrm{m}}) = (3/2)(L_{\mathrm{m}}^2/Nk_{\mathrm{B}}T_{\mathrm{m}}^2)[(1/\beta\alpha)\hat{s}^{7/3}\exp\{-\beta\alpha\hat{s}^{2/3}\}]. \quad (11)$$

The normal specific heat of the crystal A-state usually includes the defects' formation energy, the anharmonic term in the lattice vibration, and the contribution from the classical Dulong–Petit value. The former two terms have linear but gentle temperature dependence. The anomalous specific heat in the vicinity of the melting point is caused by the second term on the right-hand side of (10). The size of clusters, $\hat{s}$, can be estimated by applying the above theory to ionic crystals using the experimental specific heat data and all other available experimental data. In section 3, we will show the alternative method to obtain the cluster size $\hat{s}$ from the conductivity data.

3. Conductivity of A-state and B′-clusters

Now we consider B′-state clusters with conductivity $\sigma_{\mathrm{B}'}$ and A-state clusters with conductivity σ_{A} in an ionic crystal. Our purpose is to show how the observed conductivity at the melting temperature T_{m}, i.e. $\sigma_{\mathrm{obs}}(T_{\mathrm{m}})$, can be represented. From the consideration of the dielectric constant of the spherical B′-clusters with radius r, we have the expression

$$E' = \{3\varepsilon_{\mathrm{A}}/(\varepsilon_{\mathrm{B}'} + 2\varepsilon_{\mathrm{A}})\}E_0 \quad (12)$$

where E_0 and E' are the external electrical field and that of inside of the B′-cluster, respectively; ε_{A}, and $\varepsilon_{\mathrm{B}'}$ are the dielectric constants of A-state and B′-state, respectively. Then we can obtain the following expression,

$$E' = \{3\sigma_{\mathrm{A}}/(\sigma_{\mathrm{B}'} + 2\sigma_{\mathrm{A}})\}E_0. \quad (13)$$

The electric current density in the B′-cluster is expressed as $\sigma_{\mathrm{B}'}\{3\sigma_{\mathrm{A}}/(\sigma_{\mathrm{B}'} + 2\sigma_{\mathrm{A}})\}E_0$. This fact suggests that the electric conductivity of the system at melting temperature, $\sigma_{\mathrm{obs}}(T_{\mathrm{m}})$, has been altered by the existence of the B′-clusters. Hereafter, we simply write $\sigma_{\mathrm{obs}}(T_{\mathrm{m}})$ as σ_{m}. Using (4), the fraction of ionic pairs in the 'L' clusters to the number of total ions, $x_{\mathrm{B}'}$, is written as follows,

$$x_{\mathrm{B}'} = \hat{s}g_s/N = \hat{s}\exp[-\beta\{s(\mu_{\mathrm{B}} - \mu_{\mathrm{A}}) + \alpha s^{2/3}\}] \quad (14)$$

then σ_{m} is expressed as

$$\sigma_{\mathrm{m}} = (1 - x_{\mathrm{B}'})\sigma_{\mathrm{A}} + x_{\mathrm{B}'}\{3\sigma_{\mathrm{A}}\sigma_{\mathrm{B}'}/(\sigma_{\mathrm{B}'} + 2\sigma_{\mathrm{A}})\} \quad (15)$$

$$= [1 - \hat{s}\exp\{-\beta(\alpha\hat{s}^{2/3})\}]\sigma_{\mathrm{A}} + \hat{s}\exp\{-\beta(\alpha\hat{s}^{2/3})\} \times \{3\sigma_{\mathrm{A}}\sigma_{\mathrm{B}'}/(\sigma_{\mathrm{B}'} + 2\sigma_{\mathrm{A}})\}. \quad (16)$$

The large deviation of the electric conductivities from linearity in the high temperature region in ionic crystals is experimentally observed. If we use the observed value of the crystal at T_{m} as σ_{m}, the extrapolated value at T_{m} as σ_{A}, and the value in molten phase at T_{m} as $\sigma_{\mathrm{B}'}$, and put them into (16), then we can obtain the number of ion pairs in the B′-clusters, $\hat{s}$.

We can obtain a different expression for the ionic conductivity by a different model. The effective medium approximation (EMA) is applied to the macroscopic random mixing state [19]. As discussed above, we assume that the system is random mixture of two different states, the A-state and B′-state, with dielectric constants ε_{A} and $\varepsilon_{\mathrm{B}'}$, respectively. We consider the case that there is a sphere of A-state in the effective medium with electric constant ε_{m}. The magnitude of the polarization per unit volume in the A-state sphere, P_{A}, induced by the external electric field E_0, is represented as

$$P_{\mathrm{A}} = \{3\varepsilon_{\mathrm{m}}(\varepsilon_{\mathrm{A}} - \varepsilon_{\mathrm{m}})/(\varepsilon_{\mathrm{A}} + \varepsilon_{\mathrm{m}})\}E_0. \quad (17)$$

Similarly, we have

$$P_{\mathrm{B}'} = \{3\varepsilon_{\mathrm{m}}(\varepsilon_{\mathrm{B}'} - \varepsilon_{\mathrm{m}})/(\varepsilon_{\mathrm{B}'} + \varepsilon_{\mathrm{m}})\}E_0 \quad (18)$$

where $P_{\mathrm{B}'}$ is the magnitude of the polarization per unit volume in the B′-state sphere in the effective medium induced by the external electric field E_0. EMA demands the conditions,

$$x_{\mathrm{A}}P_{\mathrm{A}} + x_{\mathrm{B}'}P_{\mathrm{B}'} = 0 \quad (19)$$

where $x_{\mathrm{A}} + x_{\mathrm{B}'} = 1$. Therefore, we have

$$x_{\mathrm{A}}\{(\varepsilon_{\mathrm{A}} - \varepsilon_{\mathrm{m}})/(\varepsilon_{\mathrm{A}} + \varepsilon_{\mathrm{m}})\} + x_{\mathrm{B}'}\{(\varepsilon_{\mathrm{B}'} - \varepsilon_{\mathrm{m}})/(\varepsilon_{\mathrm{B}'} + \varepsilon_{\mathrm{m}})\} = 0. \quad (20)$$

By analogy, we have

$$(1 - x_{\mathrm{B}'})\{(\sigma_{\mathrm{A}} - \sigma_{\mathrm{m}})/(\sigma_{\mathrm{A}} + \sigma_{\mathrm{m}})\} + x_{\mathrm{B}'}\{(\sigma_{\mathrm{B}'} - \sigma_{\mathrm{m}})/(\sigma_{\mathrm{B}'} + \sigma_{\mathrm{m}})\} = 0. \quad (21)$$

By putting the experimental values in (21), we can obtain $x_{\mathrm{B}'}$ and $\hat{s}$.

4. Numerical application

In the previous sections, we have discussed the premelting features of ionic crystals on the basis of the re-examined Frenkel's theory. In order to compare this to the theoretical results, we have performed MD simulation in $(K_{0.5}Na_{0.5})Cl$, $Ag(Br_{0.6}Cl_{0.4})$ and $(Ag_{0.7}Cu_{0.3})Br$ systems. The simulation procedure is essentially the same as previous works [10–14].

The Tosi–Fumi type pair potentials are used in MD for $(K_{0.5}Na_{0.5})Cl$, as [20],

$$V_{ij}(r) = B_{ij}\exp(-a_{ij}r) + z_i z_j e^2/r - C_{ij}/r^6 \qquad (22)$$

where the first term represents the short range repulsion between ions; the second term stands for the Coulomb interactions with the charge of ions, z_i and z_j; and the third term represents the van der Waals interactions.

For $Ag(Br_{0.6}Cl_{0.4})$ and $(Ag_{0.7}Cu_{0.3})Br$, Rahman, Vashishta and Parrinello (RVP) [21] type potentials are used, which are written as

$$V_{ij}(r) = H_{ij}/r^{nij} + z_i z_j e^2/r - P_{ij}/r^4 - C_{ij}/r^6 \qquad (23)$$

where the first term stands for the repulsion between ions; the second term is the Coulomb interaction; the third term are the charge–dipole interactions; and the fourth term is the van der Waals contribution. The adopted parameter values are taken from the literature [22, 23]. The MD calculations are carried out for $(K_{0.5}Na_{0.5})Cl$, $Ag(Br_{0.6}Cl_{0.4})$ and $(Ag_{0.7}Cu_{0.3})Br$ using 8000 atoms (4000 cations and 4000 anions) placed in a cubic cell. The number of ions in the MD cell is decided so that it will include the whole 'L' cluster estimated by the theory. The periodic boundary condition for the MD cell, and the Ewald method for the calculation of Coulomb interaction are used. The cell is equilibrated at constant temperature, and subsequently the MD calculation is carried out on the condition that the number of particles, the volume of the cell, and the total energy of the system (NVE) are constant.

The Lindemann instability criterion was introduced in order to detect distorted particles in a recent MD study on the Lennard-Jones (LJ) crystal [17, 24]. In this study, we have also evaluated the Lindemann ratio δ_L, which is calculated from the root-mean-square displacement of the particle i at a position $\mathbf{r}_i(t)$ from its original lattice site $\mathbf{R}_i(0)$, i.e. $\langle\Delta\mathbf{r}^2\rangle^{1/2} = \langle(\mathbf{r}_i(t) - \mathbf{R}_i(0))^2\rangle^{1/2}$, divided by the average nearest neighbor distance $\langle\mathbf{r}_{kl}\rangle$. The values of δ_L are calculated at the temperatures corresponding to the molten phase at 100 K above the melting point, at the melting point, and to the solid phase at 100 K below the melting point. The calculation of δ_L is performed during 1000 MD steps. One MD time step is 2.0×10^{-15} s.

We adopt the critical Lindemann ratio, $\delta c > 0.24$, in order to distinguish 'Lindemann particles', which we have referred to as 'quasi-liquid' or 'L' particles in previous sections, from 'solid-like' particles or 'S' particles. The estimated numbers of 'L' particles at melting point of $(K_{0.5}Na_{0.5})Cl$ crystals are 204 K, 732 Na and 1199 Cl; $Ag(Br_{0.6}Cl_{0.4})$, 2295 Ag, 388 Br and 254 Cl; $(Ag_{0.7}Cu_{0.3})Br$, 1320 Ag, 1200 Cu and 341 Br, respectively. The average of δ_L calculated during 1000 MD steps are listed in table 1 for 'L' and 'S' ions in $(K_{0.5}Na_{0.5})Cl$, $Ag(Br_{0.6}Cl_{0.4})$ and $(Ag_{0.7}Cu_{0.3})Br$ at 930 K, 686 K and 613 K, respectively. The estimated margin of error is ± 0.004.

The obtained average δ_L for 'L' ions of K, Na, Cl and Br is about 0.26–0.27, whereas, the average δ_L for 'L' ions of Ag and Cu are 0.32 and 0.58, respectively. This fact indicates the mobile feature of noble metal 'L' ions, in particular Cu ions move widely, so all Cu ions are classified as 'L' ions.

Table 1. Average of δ_L for 'L' and 'non L' ions.

$(K_{0.5}Na_{0.5})Cl$ at 930 K	δ_L	$Ag(Br_{0.6}Cl_{0.4})$ at 686 K	δ_L	$(Ag_{0.7}Cu_{0.3})Br$ at 613 K	δ_L
'L' K ions	0.26	'L' Ag ions	0.31	'L' Ag ions	0.33
'L' Na ions	0.27	'L' Br ions	0.26	'L' Cu ions	0.58
'L' Cl ions	0.27	'L' Cl ions	0.26	'L' Br ions	0.26
'S' ions	0.21	'S' ions	0.19	'S' ions	0.19

Some of the typical examples of trajectories of ions will be helpful for understanding the configuration difference of ions, which are drawn to 1000 MD time steps. The trajectories of 'L' type cations, K and Na, and anions, Cl, in $(K_{0.5}Na_{0.5})Cl$, projected on the x–y plane, are shown in figures 1(a), and (b), respectively. Cluster-like structures are clearly seen in these figures. For $Ag(Br_{0.6}Cl_{0.4})$, as is seen in figure 2(b), the anions, Br and Cl, form a cluster-like distribution, which resembles those of the 'L' ions in $(K_{0.5}Na_{0.5})Cl$. As seen in figure 2(a), the trajectories of Ag ions in $Ag(Br_{0.6}Cl_{0.4})$ show a more extensive distribution, and cluster-like distributions are also observed. As mentioned in section 1, the transition to the superionic phase in the Ag–halide mixture $Ag(Br_{0.6}Cl_{0.4})$ at high temperature also seems to be prevented by melting, which is experimentally observed in AgBr [8, 9]. On the other hand, as seen in figures 1(c) and 2(c), 'S' ions in both $(K_{0.5}Na_{0.5})Cl$ and $Ag(Br_{0.6}Cl_{0.4})$ move around their crystal lattice points, corresponding to the small δ_L value of solid phase. These facts show the propriety of the calculation separating ions by δ_L. In the $(Ag_{0.7}Cu_{0.3})Br$ system, as seen in figures 3(a) and (c), the trajectories of Ag and Br 'L' ions resemble those of Ag and anions in $Ag(Br_{0.6}Cl_{0.4})$. As seen in figure 3(b), however, the trajectory of Cu ions is more diffusive than Ag and Br in $(Ag_{0.7}Cu_{0.3})Br$. According to the experiment, Cu ions have a tendency to go into the interstitial position from their initial rock salt lattice site [25]. The simulation results of the trajectory of Cu ions show the liquid-like features of Cu ions, which corresponds to the experimental results.

Next, as case studies for pseudo-binary ionic crystals, we will estimate some quantitative magnitudes of the 'L' clusters of $Ag(Br_{0.6}Cl_{0.4})$, $(K_{0.5}Na_{0.5})Cl$ and $(Ag_{0.7}Cu_{0.3})Br$ by the theory considered in the previous sections and the results of MD.

(a) *Case study for* $(K_{0.5}Na_{0.5})Cl$

We will deal with the conductivity of $(K_{0.5}Na_{0.5})Cl$, because there is no available experimental data on the temperature dependence of the specific heat of $(K_{0.5}Na_{0.5})Cl$, as far as we know, which requires the use of (11) to obtain $\hat{s}$. According to the experimental conductivity data in the solid phase, we obtain the conductivity at melting point by extrapolation as $\sigma_m = 3.24 \times 10^{-4}\ \Omega^{-1}\ \mathrm{cm}^{-1}$ [26]. We use the data in the molten phase at the melting temperature, $\sigma_{B'} = 2.18\ \Omega^{-1}\ \mathrm{cm}^{-1}$ for that of B′-state [27]. It is known that both cations and anions affect the electric conductivity of ionic crystals in the high temperature region. In this case, the intrinsic electric conductivity of alkali–halide crystals

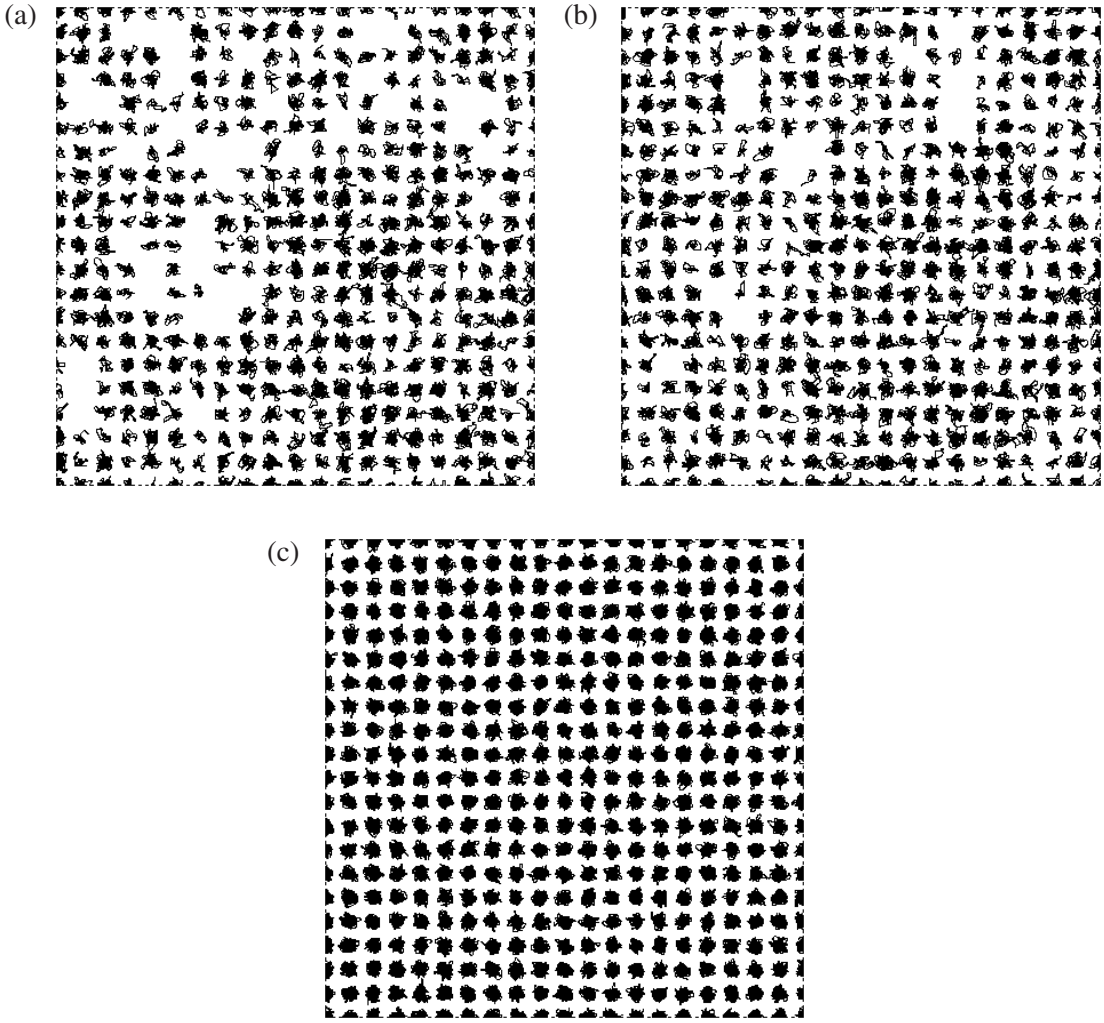

Figure 1. Trajectories of (a) K and Na 'L', (b) Cl 'L' and (c) K, Na and Cl 'S' ions in $(K_{0.5}Na_{0.5})Cl$ at 930 K.

is expressed as

$$\sigma_A T = \sigma_c T + \sigma_a T = C_0 \exp(-W_c/k_B T) + A_0 \exp(-W_c/k_B T). \quad (24)$$

Fuller and Reilly [28] evaluated the parameters in (24) for alkali chlorides. We use the average values of NaCl and KCl for σ_A. Putting the data into the first model (16) with $\beta\alpha \sim 1/7$, we obtain $\hat{s} \sim 1100$. On the other hand, by the second model (21), we obtain $\hat{s} \sim 800$. These theoretical $\hat{s}$ numbers seem to be comparable to the MD result $\hat{s} = 1067$.

(b) *Case study for* $Ag(Br_{0.6}Cl_{0.4})$

The conductivities of the solid and liquid phase at the melting temperature, estimated from experiments, are $\sigma_m = 0.429\ \Omega^{-1}\ cm^{-1}$ and $\sigma_{B'} = 3.04\ \Omega^{-1}\ cm^{-1}$, respectively [29, 30]. Using the calculated data for σ_A [31], we obtain $\hat{s} \sim 1500$ by (16) and (21). Unfortunately, as far as we know, there is no available data on the latent heat and the temperature dependence of specific heat for $Ag(Br_{0.6}Cl_{0.4})$, so we postulate that the latent heat and the deviation of specific heat from linearity at the melting temperature are expressed as a linear combination of those of AgBr and AgCl at their melting point [16]. The estimated values are $\Delta C_p = 5.0\ cal\ mol^{-1}\ K^{-1}$, and $L_m = 2.58 \times 10^3\ cal\ mol^{-1}$. Putting these values into (11) using $\beta\alpha \sim 1/7$, we also obtain $\hat{s} \sim 1650$, which is comparable to the average value of 1470 obtained by MD. The MD result is reproduced by $\beta\alpha \sim 1/6.6$.

(c) *Case study for* $(Ag_{0.7}Cu_{0.3})Br$

The specific heat of solid $(Ag_{0.7}Cu_{0.3})Br$ to the melting point has been obtained by an experimental study [32]. The excess specific heat ΔC_p, i.e. the deviation from the linear extrapolation from low temperature has been estimated [32]. The molar specific heat at constant pressure C_p can be expressed as $C_p = C_p^0 + \Delta C_p$, where C_p^0 involves the usual harmonic and anharmonic contributions. The estimated excess specific heat is $\Delta C_p(T_m) = 1.79\ cal\ mol^{-1}\ K^{-1}$. For the other data required in (11), we have also adopted the values; $L_m = 2.24 \times 10^3\ cal\ mol^{-1}$ estimated from the specific latent heat of AgBr and CuBr. Putting these values into (11) and using $\alpha\beta \sim 1/7$, we obtain $\hat{s} \sim 1800$, which is comparable to the average number of 'L' particle pairs,

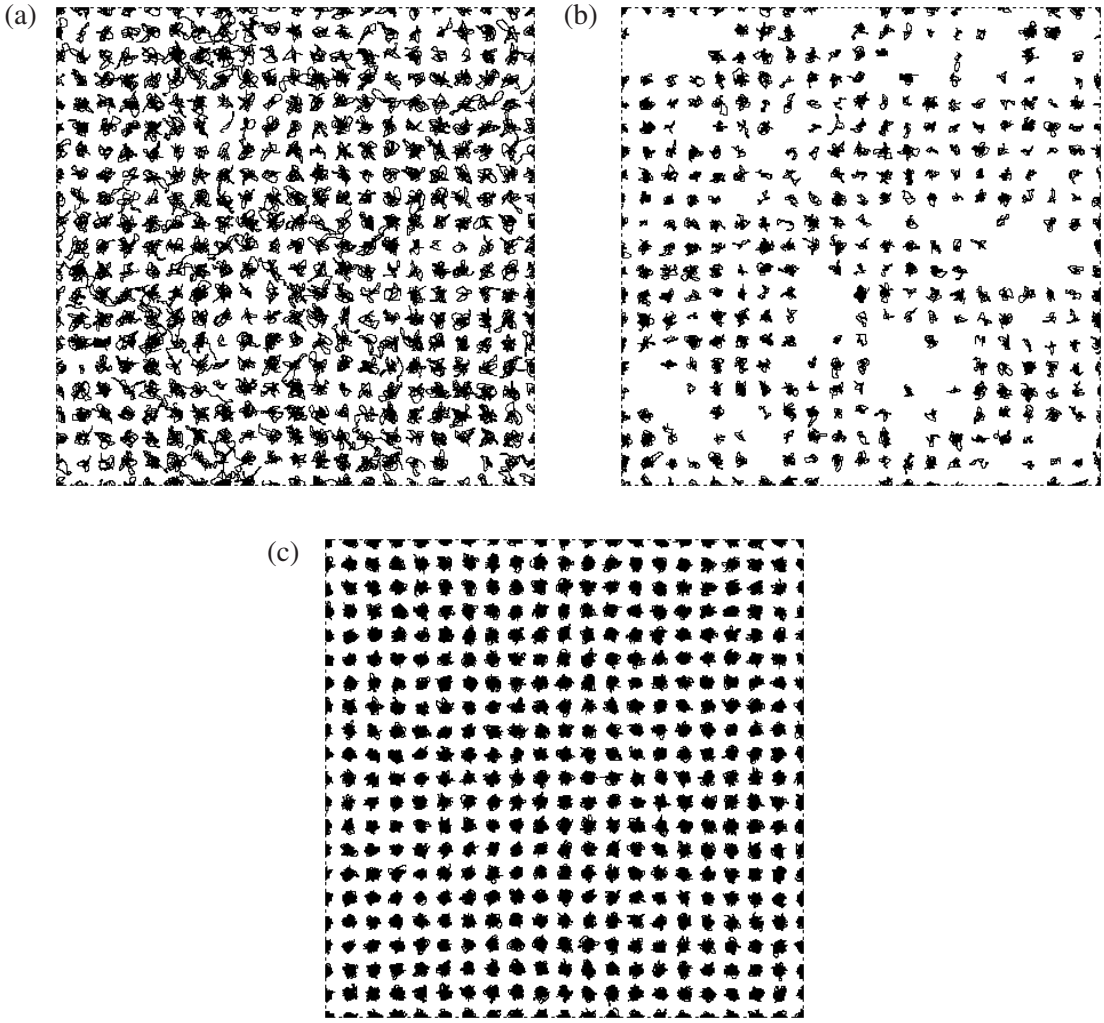

Figure 2. Trajectories of (a) Ag 'L', (b) Br and Cl 'L' and (c) Ag, Br and Cl 'S' ions in $Ag(Br_{0.6}Cl_{0.4})$ at 686 K.

1430, given by MD. The MD result is reproduced by $\beta\alpha \sim 1/6.2$.

Saito *et al* [32] have estimated the occupation probability of cations on the tetrahedral or interstitial sites for $(Ag_{0.7}Cu_{0.3})Br$ using the model of Schottky-type excess specific heat which is caused by jumps of the mobile ions between two types of sites; the octahedral site and the tetrahedral site. However, the estimated occupation probability by this model is about 25% at the melting point, which is rather small compared to the number of 'L' cations obtained by MD. This discrepancy may be assigned to the fact that the thermodynamic model of the two different energy sites has neglected the cations at the intermediate positions, and the interactions between defects. This result may suggest that the 'L' clusters in the premelting region can be detected more sensitively by the Frenkel-type defect model and the Lindemann instability condition.

5. Transport properties

In this section, we calculate the mean square displacement (MSD), $r_\xi^2(t)$, and the velocity autocorrelation functions (VAF) in order to clarify the dynamical behavior of 'L' ions and 'S' ions at the premelting temperature. We briefly summarize the procedure [33]. MSD is defined as

$$r_\xi^2(t) = \frac{1}{N_\xi}\sum_{i=1}^{N_\xi}\langle|\boldsymbol{r}_i(t) - \boldsymbol{r}_i(0)|^2\rangle_\xi \tag{25}$$

where i and N_ξ represent the ith ion of the ξ-type ion and its number, respectively. The angular brackets indicate an average over all atomic positions $\boldsymbol{r}_i(t)$ and the time average, or ensemble average. The diffusion coefficient is related to MSD as

$$D_\xi = \lim_{t\to\infty}\frac{r_\xi^2(t)}{6t}. \tag{26}$$

If t is small enough, then

$$r_\xi^2(t) \cong \langle \boldsymbol{v}_i(0)\cdot\boldsymbol{v}_i(0)\rangle_\xi t^2 = \frac{3k_\mathrm{B}t}{m_\xi}t^2. \tag{27}$$

The VAF for the ξ-type ion is defined using the velocity of the ith ion at time t, $\boldsymbol{v}_i(t)$ as

$$f_\xi(t) = \frac{1}{N_\xi}\sum_{i(\xi)}\langle \boldsymbol{v}_i(t)\cdot\boldsymbol{v}_i(0)\rangle_\xi \tag{28}$$

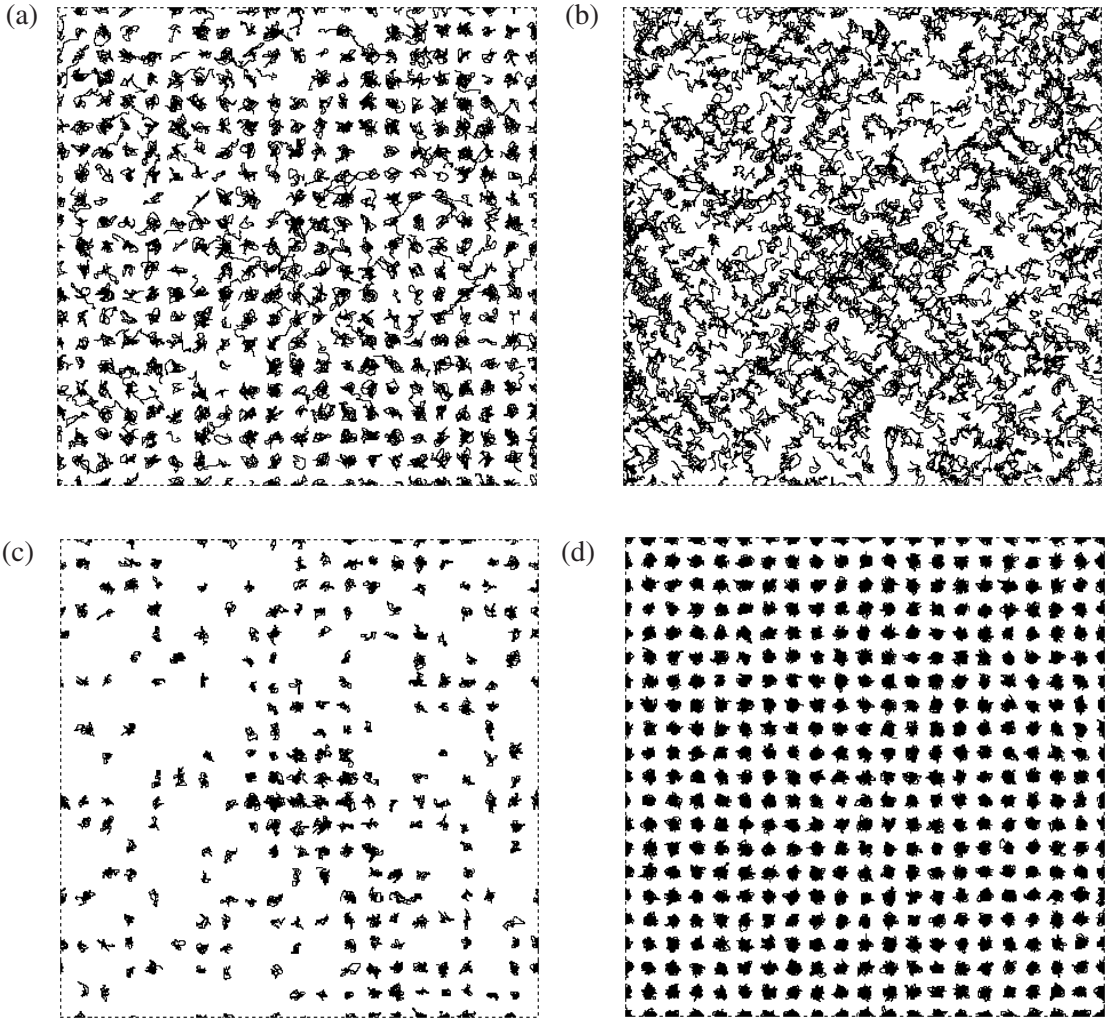

Figure 3. Trajectories of (a) Ag 'L', (b) Cu 'L', (c) Br 'L' and (d) Ag and Br 'S' ions in $(Ag_{0.7}Cu_{0.3})Br$ at 613 K.

the normalized VAF is defined as

$$\Phi_\xi(t) = \frac{f_\xi(t)}{f_\xi(0)}. \tag{29}$$

The frequency dependent diffusion coefficients $D_\xi(\omega)$ in the premelting region and molten phase are obtained to discuss the phonon mode. The Fourier transformation of $\Phi_\xi(t)$ is given by

$$\Phi_\xi(\omega) = \int_0^\infty \mathrm{d}t\ \Phi_\xi(t)\mathrm{e}^{\mathrm{i}\omega t}. \tag{30}$$

$D_\xi(\omega)$ is obtained from $\Phi_\xi(\omega)$ as

$$D_\xi(\omega) = \frac{k_\mathrm{B}T}{m_\xi}\Phi_\xi(\omega). \tag{31}$$

As $D_\xi(\omega)$ is proportional to the density of states of the normal modes in a harmonic system, it might be appropriate to compare $D_\xi(\omega)$ with experimental data of the density of states of phonons [34, 35]. The static limit value of $D_\xi(\omega)$ is related to the self-diffusion coefficient D_ξ as

$$D_\xi = \frac{k_\mathrm{B}T}{m_\xi}\Phi_\xi(\omega = 0). \tag{32}$$

In order to clarify the difference of the short time detailed behaviors of ions, the obtained MD results of $r_\xi^2(t)$ are shown in figures 4(a)–(c), with the long time results of $r_\xi^2(t)$ from $t = 0$ to 4.0×10^{-12} s in the inset. As seen in these figures, the $r_\xi^2(t)$s increase in proportion to t^2 in the vicinity of $t = 0$. The results for $(K_{0.5}Na_{0.5})Cl$ and $Ag(Br_{0.6}Cl_{0.4})$ are shown in figures 4(a) and (b), respectively, where the $r_\xi^2(t)$ of ions in the molten phase increase linearly with lapsed time, as seen in the insets, whereas the $r_\xi^2(t)$ of ions in the solid phase and the premelting region become flat over the course of time. On the other hand, for $(Ag_{0.7}Cu_{0.3})Br$, as seen in figure 4(c), not only the ions in the molten phase but also the cations in the premelting and solid phase are diffusive, i.e. the $r_\xi^2(t)$s are not flat in the inset graph. This MD result corresponds to the experimental fact that Cu ions in the solid phase of $(Ag_{0.7}Cu_{0.3})Br$ are diffusive and have a tendency to go into the interstitial site of the rock salt structure [25, 32].

As seen in figures 4(a)–(c), for a certain ion, the same order of $r_\xi^2(t)$s can be seen, i.e. $r_\xi^2(t)$ of the molten phase, 'L' and 'S', and solid phase can be seen in this order from top to bottom. Moreover, for $(K_{0.5}Na_{0.5})Cl$, the $r_\xi^2(t)$s of Na, Cl and K appear in this order from top to bottom; for $Ag(Br_{0.6}Cl_{0.4})$,

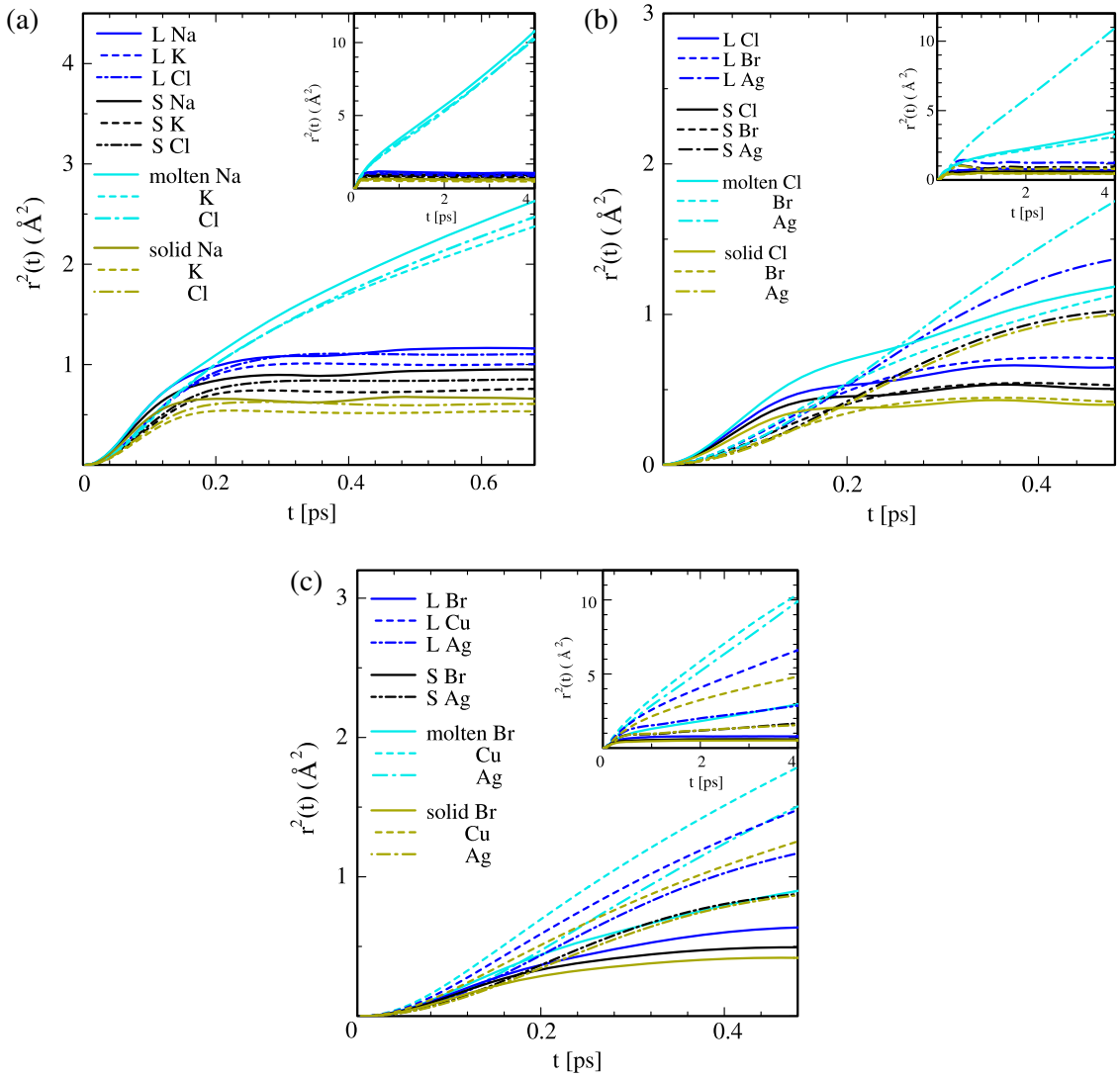

Figure 4. MSD of 'L' ions and 'S' ions in (a) $(K_{0.5}Na_{0.5})Cl$ at 930 K, (b) $Ag(Br_{0.6}Cl_{0.4})$ at 686 K and (c) $(Ag_{0.7}Cu_{0.3})Br$ at 613 K with those of the molten phase 100 K above the melting point, and the solid phase 100 K below the melting point. The graphs on a long timescale are shown as insets.

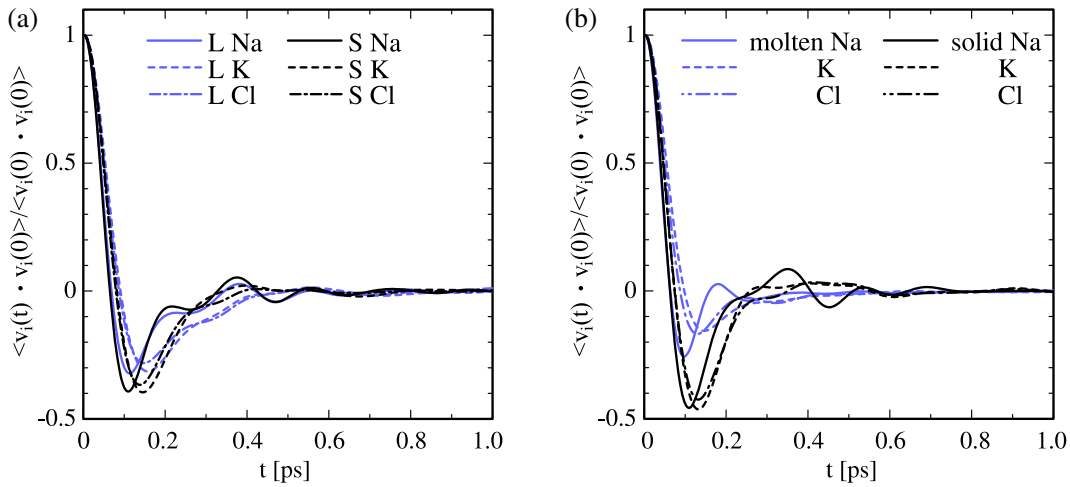

Figure 5. The normalized VAF of (a) 'L' ions and 'S' ions (black line) in $(K_{0.5}Na_{0.5})Cl$ at 930 K and (b) the molten phase 100 K above the melting point and the solid phase 100 K below the melting point (black line) in $(K_{0.5}Na_{0.5})Cl$.

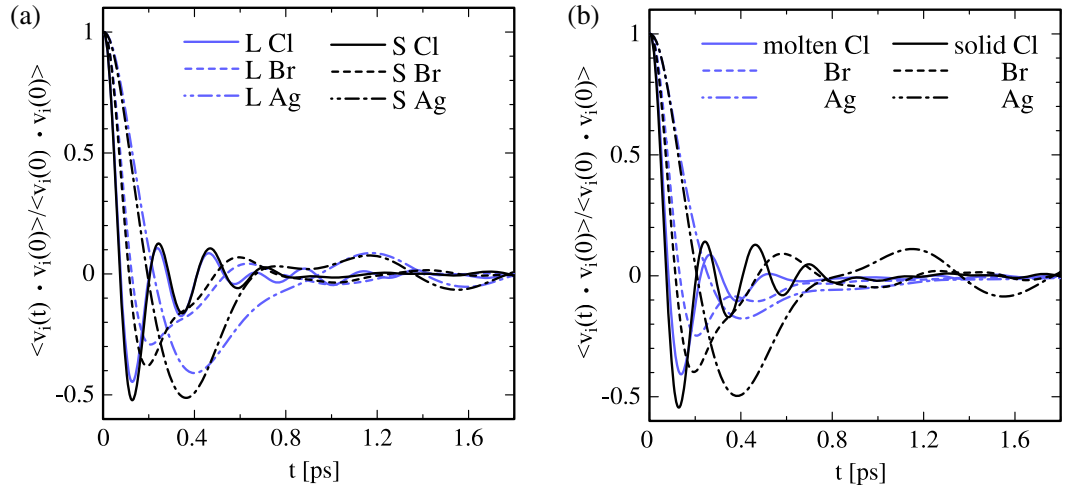

Figure 6. The normalized VAF of (a) 'L' ions and 'S' ions (black line) in $Ag(Br_{0.6}Cl_{0.4})$ at 686 K and (b) the molten phase 100 K above the melting point and the solid phase 100 K below the melting point (black line) in $Ag(Br_{0.6}Cl_{0.4})$.

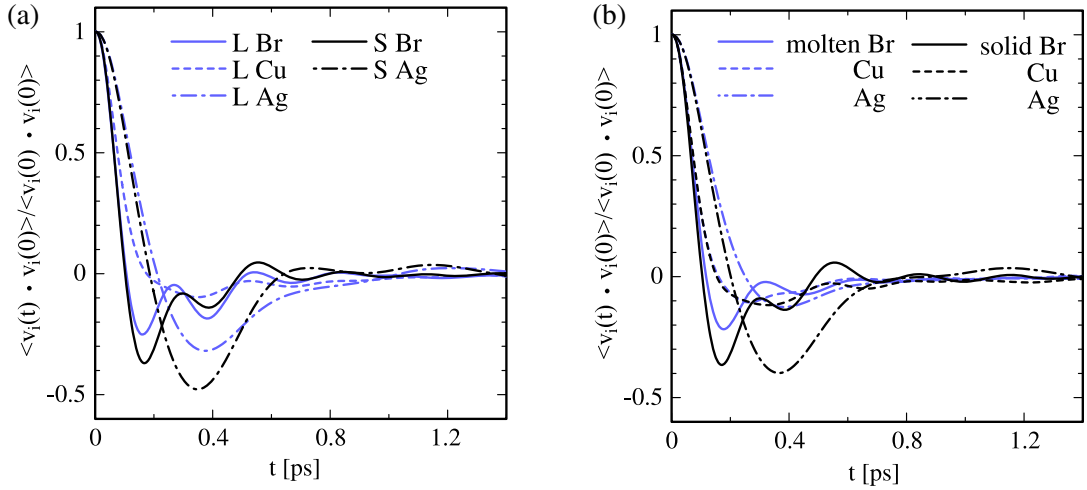

Figure 7. The normalized VAF of (a) 'L' ions and 'S' ions (black line) in $(Ag_{0.7}Cu_{0.3})Br$ at 613 K and (b) the molten phase 100 K above the melting point and the solid phase 100 K below the melting point (black line) in $(Ag_{0.7}Cu_{0.3})Br$.

the order is Ag, Cl and Br; and for $(Ag_{0.7}Cu_{0.3})Br$, the order is Cu, Ag and Br. This MD result suggests that the order of size of diffusion coefficients of the ions is the same even in different phases, which is related to the inclination of $r_\xi^2(t)$ from (26).

It is interesting to see the short time behavior in $r_\xi^2(t)$ for the 'L' ions in figures 4(a)–(c). As seen in figure 4(a) for $(K_{0.5}Na_{0.5})Cl$, the $r_\xi^2(t)$s of 'L' ions begin to separate from the increasing $r_\xi^2(t)$ lines of the molten phase at approximately 1.5×10^{-13} s; for $Ag(Br_{0.6}Cl_{0.4})$ in figure 4(b), the $r_\xi^2(t)$s of the 'L' ions begin to separate from the lines of the molten phase approximately from 1.2×10^{-13} to 4.0×10^{-13} s; and for $(Ag_{0.7}Cu_{0.3})Br$ in figure 4(c), the separation begins from 1.6×10^{-13} to 3.8×10^{-13} s. The short time behavior of the $r_\xi^2(t)$s seem to be related to the minimum of their VAF, which are shown in figures 5(a)–7(b). As seen in figure 5(a), the VAF of the 'L' ions of $(K_{0.5}Na_{0.5})Cl$ has minima at 1.2×10^{-13}, 1.4×10^{-13} and 1.5×10^{-13} s, corresponding to their MSD; for $Ag(Br_{0.6}Cl_{0.4})$ in figure 6(a), the minima are at 1.2×10^{-13}, 2.0×10^{-13} and 4.0×10^{-13} s; for $(Ag_{0.7}Cu_{0.3})Br$ in figure 7(a), the minima are at 1.6×10^{-13}, 3.6×10^{-13} and 3.8×10^{-13} s. These large negative values at the deep minima of the VAF are interpreted as the back-scattering or 'rattling' motion of ions in a cage of neighboring ions [36]. A difference of the depth of the minimum of the VAF between the 'L' and 'S' ions can be clearly observed, i.e. the minima of the 'L' ions are shallower than those of the 'S' ions. This fact indicates that 'L' ions are more diffusive than 'S' ions. As seen in figures 5(a)–7(b), however, the difference of the VAF between 'L' and 'S' ions is not as conspicuous as that between the molten and solid phase.

The $D_\xi(\omega)$s are obtained from VAF by (30) and (31). As seen in figures 8(a)–10(b), the $D_\xi(\omega)$s have pronounced peaks in the infrared, i.e. 'terahertz' region, which is characterized by its extraordinary features, e.g. strong permeability into substances [37]. As seen in figures 8(a) and (b) for $(K_{0.5}Na_{0.5})Cl$, the two split peaks of $D_\xi(\omega)$ for Na in the premelting region and the solid phase corresponding to longitudinal acoustic (LA) and longitudinal optic (LO) phonon modes are observed [38]. As seen in figures 9(a)–10(b), similar

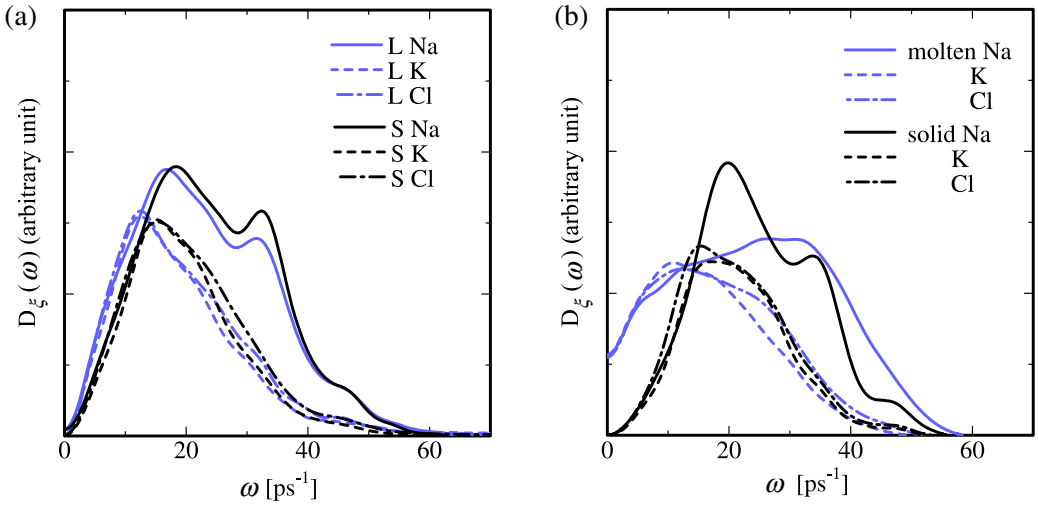

Figure 8. (a) $D_\xi(\omega)$ of 'L' ions and 'S' ions (black line) in $(K_{0.5}Na_{0.5})Cl$ at 930 K. (b) $D_\xi(\omega)$ of the molten phase 100 K above the melting point and the solid phase 100 K below the melting point (black line) in $(K_{0.5}Na_{0.5})Cl$.

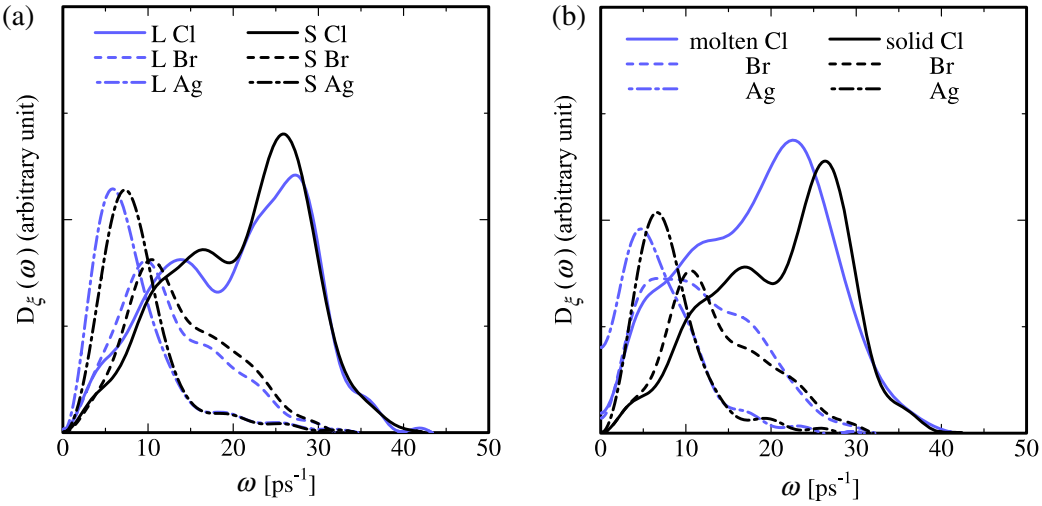

Figure 9. (a) $D_\xi(\omega)$ of 'L' ions and 'S' ions (black line) in $Ag(Br_{0.6}Cl_{0.4})$ at 686 K. (b) $D_\xi(\omega)$ of the molten phase 100 K above the melting point and the solid phase 100 K below the melting point (black line) in $Ag(Br_{0.6}Cl_{0.4})$.

two splits can be seen in the $D_\xi(\omega)$s of Cl in $Ag(Br_{0.6}Cl_{0.4})$, and Br in $(Ag_{0.7}Cu_{0.3})Br$ for the premelting and solid phases, respectively.

As seen in these figures, the $D_\xi(\omega)$ peaks of the 'L' ions are broadened and observed at lower frequencies than those of the 'S' ions, which can be interpreted as a more diffusive feature, or softness, of the 'L' ion cluster, though these tendencies in the $D_\xi(\omega)$ peaks are more obvious in the difference between the molten and solid phases. It seems interesting to find the exception that the second peak of $D_\xi(\omega)$, i.e. the LO mode of the Cl 'L' ion in $Ag(Br_{0.6}Cl_{0.4})$ in figure 9(a), and that of the Br 'L' ion in $(Ag_{0.7}Cu_{0.3})Br$ in figure 10(a) appears at a slightly higher frequency than that of the 'S' ion, which contradicts the expected softness of the 'L' ions. This result might be attributed to the influence of vibrations of cations and/or the 'cage' effect from surrounding ions, however, the detailed explanation remains for future analysis.

6. Conclusion

The theory of the premelting phenomena in ionic crystals on the basis of the concept of the heterophase fluctuation, which is connected with specific heat and conductivity, has been applied to the pseudo-binary ionic crystals in the KCl–NaCl, AgBr–AgCl and AgBr–CuBr systems.

MD has been performed to examine the ionic configurations in their premelting region in the vicinity of their melting points. Liquid-like clusters have been observed in the results of MD utilizing the Lindemann instability condition. The size of the liquid-like clusters has been estimated by theory and MD, and they are in good agreement with each other.

The characteristic dynamic and transport properties of liquid-like clusters in the premelting region have also been discussed by MSD and VAF. The results show obvious differences between the 'L' and 'S' ions in their structural and transport properties. 'L' ions show intermediate features

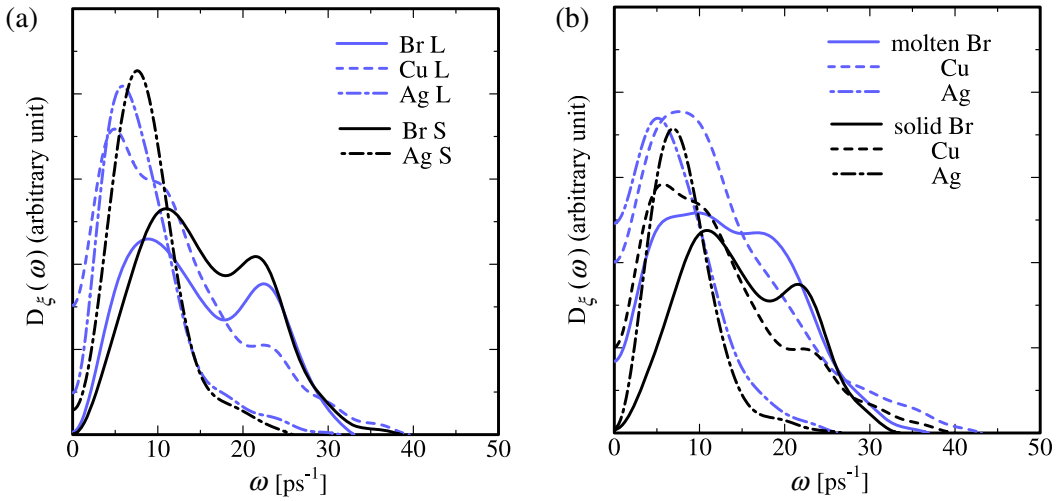

Figure 10. (a) $D_\xi(\omega)$ of 'L' ions and 'S' ions in $(Ag_{0.7}Cu_{0.3})Br$ at 613 K. (b) $D_\xi(\omega)$ of the molten phase 100 K above the melting point (blue line) and the solid phase 100 K below the melting point (black line) in $(Ag_{0.7}Cu_{0.3})Br$.

between the solid and molten state. It is interesting that the characteristic features of 'L' and 'S' ions are observed more in the short time behavior in MSD and VAF.

Acknowledgments

The author wishes to express his cordial thanks to Professor S Tamaki, Professor P S Salmon and Dr M Kusakabe, for fruitful discussions and encouragement in this study. The author also expresses his thanks to the Ministry of Education, Science and Culture for financial support of a Grant-in-Aid for Science Research. Part of the simulation results in this research were obtained using the super computing resources at the Cybermedia Center, Osaka University.

References

[1] See for examples: Green P F 2005 *Kinetics, Transport, and Structure in Hard and Soft Materials* (London: Taylor and Francis)
Chiang Y-M, Birnie D P and Kingery W D 1997 *Physical Ceramics: Principles for Ceramic Science and Engneering* (New York: Wiley)
[2] Jost W and Kubaschewski P 1968 *Z. Phys. Chem. Neue Folge* **60** 69
Christy R W and Lawson A W 1951 *J. Chem. Phys.* **19** 517
Kanzaki H 1951 *Phys. Rev.* **81** 884
[3] Lawson B R 1963 *Acta Crystallogr.* **16** 1163
[4] Yamamoto S, Ohno I and Anderson O L 1987 *Phys. Chem. Solids* **48** 143
Hughes W C and Cain L S 1996 *Phys. Rev.* B **53** 5174
Cain L S and Hu G 2001 *Phys. Rev.* B **64** 104104
[5] Frenkel J 1939 *J. Chem. Phys.* **7** 200
Frenkel J 1939 *J. Chem. Phys.* **7** 538
Frenkel J 1946 *Kinetic Theory of Liquids* (Oxford: Clarendon)
[6] Matsunaga S and Tamaki S 2008 *J. Phys.: Condens. Matter* **20** 114116
Matsunaga S and Tamaki S 2008 *Eur. Phys. J.* B **63** 417
[7] See for example, Chandra S 1981 *Superionic Solids* (Amsterdam: North-Holland)
[8] Andreoni W and Tosi M P 1983 *Solid State Ion.* **11** 49
[9] Nield V M, Keen D A, Hayes W and McGreevy R L 1992 *J. Phys.: Condens. Matter* **4** 6703
[10] Matsunaga S and Madden P A 2003 *J. Phys.: Condens. Matter* **16** 181
Matsunaga S 2005 *Solid State Ion.* **176** 1929
[11] Koishi T, Kawase S and Tamaki S 2002 *J. Chem. Phys.* **116** 3018
Koishi T and Tamaki S 2004 *J. Chem. Phys.* **121** 333
Matsunaga S, Koishi T and Tamaki S 2007 *Mol. Simul.* **33** 613
[12] Matsunaga S, Saito M, Koishi T and Tamaki S 2007 *Mol. Simul.* **33** 153
Matsunaga S, Saito M, Koishi T and Tamaki S 2008 *J. Alloys Compounds* **452** 182
[13] Matsunaga S 2009 *Prog. Theor. Phys. Suppl.* **178** 113
[14] Matsunaga S 2009 *J. Phys.: Conf. Ser.* **144** 012011
[15] Kurosawa T 1957 *J. Phys. Soc. Japan* **12** 338
[16] Hainovsky N and Maier J 1995 *Phys. Rev.* B **51** 15789
[17] Jin Z H, Gumbsch P, Lu K and Ma E 2001 *Phys. Rev. Lett.* **87** 55703
[18] Egelstaff P A and Widom B 1970 *J. Chem. Phys.* **53** 2667
[19] Landauer R 1978 *Electrical Transport and Optical Properties of Inhomogeneous Media* (*AIP Conf. Proc.* vol 40) ed J C Gardland and D B Tanner (New York: AIP) pp 2–45
[20] Sangster M J L and Dixon M 1976 *Adv. Phys.* **25** 247
[21] Parrinello M, Rahman A and Vashishta P 1983 *Phys. Rev. Lett.* **50** 1073
[22] Larsen B, Førland T and Singer K 1973 *Mol. Phys.* **26** 1521
[23] Tasseven Ç, Trullàs J, Alcaraz O, Silbert M and Giro A 1997 *J. Chem. Phys.* **106** 7286
[24] Lindemann F A 1910 *Phys. Z.* **11** 609
[25] Saito M, Takahashi H and Tamaki S 1989 *J. Phys. Soc. Japan* **58** 527
[26] Erofeev V N and Hartmann E 1988 *Solid State Ion.* **23–30** 241
[27] Van Artsdalen E R and Yaffe I S 1955 *J. Phys. Chem.* **59** 118
[28] Fuller R G and Reilly M H 1967 *Phys. Rev. Lett.* **19** 113
[29] Cain L S and Slifkin L M 1980 *J. Phys. Chem. Solids* **41** 173
[30] Harrap B S and Heymann E 1955 *Trans. Faraday Soc.* **51** 259
[31] Aboagye J K and Friauf R J 1975 *Phys. Rev.* B **11** 1654
[32] Saito M, Takahashi H and Tamaki S 1989 *J. Phys. Soc. Japan* **58** 4041
[33] Hansen J-P and McDonald I R 2006 *Theory of Simple Liquids* 3rd edn (Amsterdam: Academic)
[34] Balucani U and Zoppi M 1994 *Dynamics of the Liquid State* (Oxford: Clarendon)
[35] Bruesch P 1982 *Phonons: The Theory and Experiments I* (*Springer Series on Solid-State Sciences* vol 34) (Berlin: Springer)
[36] Trullàs J, Giró A and Silbert M 1990 *J. Phys.: Condens. Matter* **2** 6643
[37] Nishizawa J 2005 *Terahertz Wave* (Tokyo: Kogyo Chosakai)
[38] March N H and Tosi M P 1976 *Atomic Dynamics in Liquids* (London: Macmillan)